The Synthesis of Copper-doped Hematite Nanoparticles of Iron Ore through Impregnation Method for Photodegradation of Textile Dyes

The Synthesis of Copper-doped Hematite Nanoparticles of Iron Ore through Impregnation Method for Photodegradation of Textile Dyes

S Lubis*, Khairi, I H Al Haitami, Murisna

Department of Chemistry, Faculty of Mathematics and Natural Sciences, Universitas Syiah Kuala, Banda Aceh 23111, Indonesia

*Corresponding author: suryalubis@unsyiah.ac.id

Abstract. Copper-doped hematite (Cu-doped α-Fe_2O_3) nanoparticles have been synthesized by the impregnation method using iron ore as the hematite source. The structural and morphological properties of the prepared samples were studied using X-ray diffraction (XRD), scanning electron microscopy (SEM), and nitrogen adsorption-desorption. The XRD results showed that the hematite extracted from iron ore was in the hematite phase. The average crystallite size of copper-doped hematite was slightly smaller than that of hematite. The copper-doped hematite nanoparticles exhibited high photocatalytic activity on degradation of indigo carmine (IC) dye with the degradation percentage of 98.21 % and 99.78%, respectively under UV and solar light irradiation. The highest photocatalytic activity was obtained at the experimental condition namely initial pH of IC solution 1.0, photocatalyst mass of 400 mg, initial concentration dye solution of 15 mg/L, and 90 minutes of irradiation times. The copper-doped hematite nanoparticles could also remove dyes found in batik wastewater with a percentage of the degradation up to 77.56 % and 97.83% under UV and solar light irradiation, respectively.

Keywords: copper, hematite, indigo carmine, photodegradation, impregnation

1. Introduction

Hematite (α-Fe_2O_3) is a promising semiconductor that can be used as photocatalyst because of the narrow bandgap (1.9-2.2 eV), chemical stability, the abundance, and low cost. Moreover, hematite collects up to 40% of the energy of solar spectrum, absorbs light up to 600 nm, and is stable in aqueous solutions [1-3]. However, the application of hematite has been limited due to the poor absorptivity, poor conductivity, rapid electron, and hole recombination after the photo-excitation of hematite [4-6]. These disadvantages could be overcome by controlled morphological synthesis of α-Fe_2O_3, surface modification, the formation of composites, and/or by doping of α-Fe_2O_3 with transition metal ions [7-8]. The structural properties of hematite are affected by the degree of crystallinity [9], particle size [10-11], and doping [12]. Doping of metal ion strongly influences the morphology, chemical reactivity, particle size, and redox behavior of Fe_2O_3. Therefore, the doping process can provide a desirable photocatalytic activity for Fe_2O_3.

Some transitions of metal ion doping photocatalyst have been reported including cobalt-doped Fe_2O_3 photocatalyst prepared by coprecipitation method that has been studied for degradation of pararosaniline dye [13]. Gallium-doped α-Fe_2O_3 with enhanced photocatalytic removal efficiency of methyl orange prepared by coprecipitation method also has been reported [14]. The purpose of this work was to synthesize 8% copper-doped hematite nanoparticles using impregnation method and study the physicochemical properties. The hematite nanoparticles were prepared from iron ore by a co-precipitation method using ammonium hydroxide and doping with copper ion by the impregnation method. The photocatalytic activity of copper-doped hematite was studied on photodegradation of indigo carmine (IC) dye that has been widely used in the textile industry. The initial pH of IC dye solution, photocatalyst mass, and initial concentration of IC effect on the photodegradation efficiency were also evaluated to set up the optimal working conditions of copper-doped hematite. The results were compared with those obtained using undoped hematite.

2. Methods

2.1. Preparation of Copper-doped Hematite

Iron ore found in Aceh Besar district, Aceh province, Indonesia was ground to reduce the particle size in a ball mill (Planetary mill, Fritch, P6) for 2 hours. Fine powder of iron ore was manually separated using a magnetic bar and sieved with a 150-mesh standard sieve. Iron compounds of iron ore were dissolved in 100 ml of 6 M HCl solution and heated at 80 °C for 2 hours. After filtering the mixture, NH_4OH was added to the filtrate solution until the pH reaches ~6 at which the iron (III) hydroxide precipitate was formed. The precipitated was filtered, washed, followed by drying at 100 °C and fired at 700 °C for 5 hours at which transformed into hematite (α-Fe_2O_3). Copper doped hematite was prepared by impregnating hematite with copper nitrate three hydrate solution ($Cu(NO_3)_2 \cdot 3H_2O$), concentration such that solids containing 8% copper was obtained. The mixture was stirred for 30 minutes and heated at 80 °C. The product obtained was dried at 100 °C for 5 hours, followed by calcination at 700 °C for 5 hours.

2.2. Characterization of Cu-doped Hematite

The crystallographic structure and phase identification of samples were determined using powder X-ray diffractometer (Shimadzu, XRD D6000), equipped with Cu-Kα radiation (40 kV, 30 mA), a scan speed 10° min^{-1} and a monochromator at a 2θ angle 10° to 80°. The Debye-Scherer's formula (Equation 1) was used to calculate the average crystallite sizes of materials (D), where D is the average crystallite size, k = 0.9 (Scherrer's constant), λ = 1.5405 Å, is the wavelength of X-ray diffraction radiation, θ is the Bragg's angle and FWHM is the full width at half maximum observed from XRD pattern [15].

$$D = \frac{k\lambda}{FWHM\cos\theta} \quad (1)$$

Scanning electron microscopy (SEM; model JSM6510LV) was used to investigate the morphology of the synthesized samples at an accelerating voltage of 15 kV. The average pore radius and specific surface area of samples were determined using a Quantachrome Nova 3200E instrument utilizing the Brunauer-Emmet-Teller (BET) method. The sample tubes were loaded with 0.1 – 0.15 g of undoped or copper doped hematite samples, then degassed in a nitrogen flow.

2.3. Photocatalytic evaluation of Cu-doped Hematite

The photocatalytic activity of Cu-doped hematite was evaluated by photodegradation experiments using indigo carmine (IC) dye under UV irradiation conditions. The experiments were conducted at room temperature on the different initial pH of the dye solution, photocatalyst mass, initial concentration of IC solution and irradiation times. Hydrochloric acid or sodium hydroxide solution was added to the IC solution to adjust the pH at the desired value measured using a pH meter

(HANNA instruments pHep). In each experiment, a certain amount of photocatalyst and 25 mL of IC solution with the definite concentration were put into a Pyrex glass vessel. The suspension was stirred for 30 min in the dark to establish the adsorption-desorption equilibrium between the photocatalyst and IC, then irradiated under UV light (6 W UV lamp, λ= 365 nm) which was placed 10 cm from the Pyrex glass vessel. A certain quantity of the IC suspension was taken at regular intervals during the irradiation period and centrifuged at 4000 rpm for 10 minutes. The residual IC dye in the solution was analyzed at λ_{max} of 610 nm by using a UV-Vis spectrophotometer (Shimadzu UV mini 1240). The percentage of IC degradation (%D) was determined by using the formula of Equation (2).

$$\text{IC Removal } \% = \frac{(C_o - C_t)}{C_o} \times 100\% \qquad (2)$$

where C_o and C_t are the initial concentration of IC and concentration of IC after irradiation time (t), respectively.

3. Results and Discussion

3.1. Characterization

Figure 1 shows XRD patterns of iron ore, undoped and 8% Cu-doped hematite nanoparticles. The diffraction peaks in iron ore corresponding to (211), (310), (311), (400), (421), and (533) planes indicated the presence of magnetite (Fe_3O_4) (Figure 1a.) according to JCPDS card no. 96-900-2317. Iron ore also contains quartz (SiO_2) and TiO_2. On the other hand, according to JCPDS card no. 96-900-9783, the diffraction peak in Figure 1b corresponded to the (110), (211), (101), (210), (202), (312), (310), and (211) reflection planes of hematite (α-Fe_2O_3). No peaks corresponding to copper oxides or copper metal that could be observed when copper was added to hematite nanoparticles exhibiting that copper had been successfully incorporated into the hematite lattice. Figure 1 also shows that the XRD patterns of undoped and copper-doped hematite almost similar suggested that incorporation of copper did not change the hematite structure. Copper doping caused the right shift in the XRD peaks position of hematite compared with undoped hematite. This observation has a good agreement with previously reported research [16-17]. Copper ion could easily substitute Fe site in Fe_2O_3 crystal lattice because the ionic radius of Cu^{2+} ion (0.073 nm) was slightly higher than that of the Fe^{3+} ion (0.065 nm). The average crystallite size of materials determined using Debye-Scherer's formula indicated that the crystallite size of Cu-doped hematite (36.16 nm) was slightly smaller in comparison with undoped hematite (36.52 nm). The crystallite size calculation was performed by measuring full-width at the half-maximum of the diffraction peaks at 2θ = 33.15°, 35.62°, and 54.08°.

SEM photographs of materials presented in Figure 2 showed that the iron ore particle had irregular and layered shape. The hematite (α-Fe_2O_3) of iron ore had two different shapes including spherical and rod-like particle (Figure 2b). The spherical shape particle had a larger size than that of rod-like shape. SEM photograph of copper-doped hematite showed no rod-like shape particle observed (Figure 2c). In addition, the spherical shape of copper-doped hematite had smaller and uniform particle size than that of hematite. Figure 2c also shows the agglomeration of Cu-doped hematite particles. This observation is in accordance with the previously reported study [13].

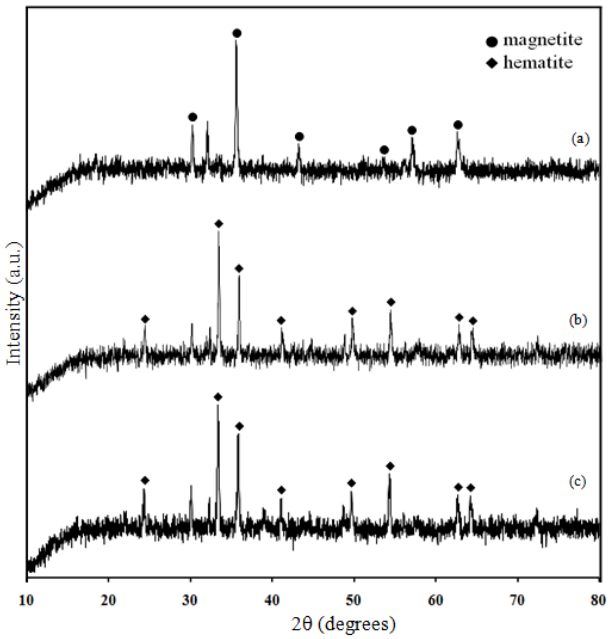

Figure 1. XRD patterns for (a) Iron ore (b) undoped and (c) Cu-doped hematite nanoparticles

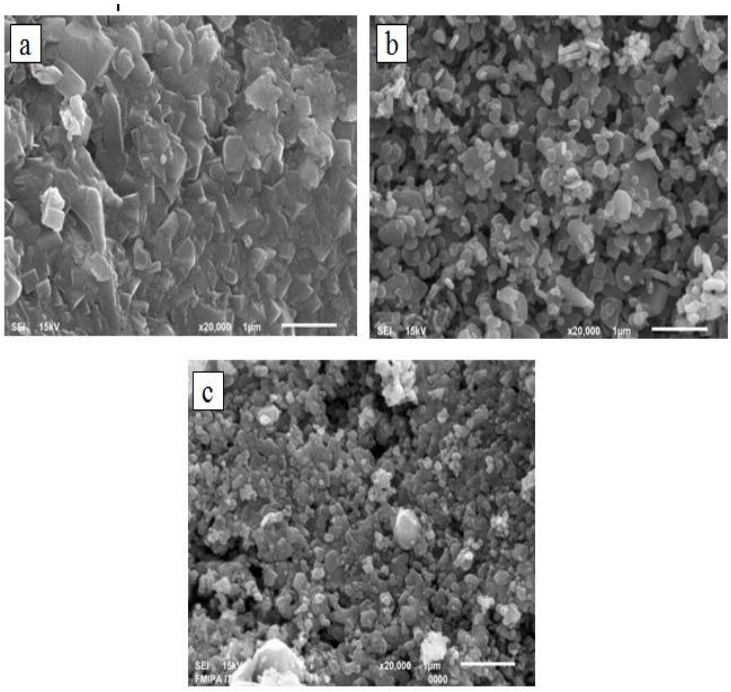

Figure 2. SEM photographs of (a) Iron ore, (b) Hematite, and (c) Cu-doped hematite

The nitrogen sorption isotherm of the materials was measured to obtain the specific surface area and the average of pore radius. As calculated by BET equation, the particular surface area of Cu-doped hematite was 7.78 m^2g^{-1}, while the undoped hematite was 5.64 m^2g^{-1}. The high surface area of Cu-doped hematite contributed to enhancing the adsorption of dye molecule on the surface of the photocatalyst. The adsorption process is an essential step on photocatalysis in the enhancement of photocatalytic activity [18]. The addition of copper ion slightly decreased the average pore radius of hematite from 3.05 nm to 2.58 nm. This observation was in in line with the crystallite size based on the XRD data.

3.2. Photocatalytic Activity

The photocatalytic activity of the Cu-doped hematite nanoparticles was investigated on the photodegradation of IC dye under UV irradiation. Figure 3 shows the effect of the initial pH of IC solution on its photodegradation. The initial pH of the IC solution was adjusted from 1 to 5; the initial IC concentration was set to 15 mg/L and the photocatalyst mass was 300 mg. The results showed an increase in photodegradation efficiency at lower pH and the highest photodegradation efficiency was achieved at pH = 1. This observation corresponded the previously reported that the maximum photodegradation of IC dye over MnO_2 occurred at pH = 2 [19] and the presence of α-ZrP occurred at pH = 3 [20].

The pH of the reaction medium affects not only the characteristics of the photocatalyst surface but also the organic dye molecules [21]. In acidic pH environment, indigo carmine as an anionic dye could be easily adsorbed on the positively charge of the surface of α-Fe_2O_3 through the negatively charged (SO_3^- group) on the IC molecule [22]. The increase in IC molecule on the photocatalyst surface led to increase the photodegradation of IC. It has been suggested that the process of dye adsorption on the surface of photocatalyst is a key factor in photodegradation [23]. The more the molecules were adsorbed, the more the number of IC molecule would react with an electron, hole, $^{\bullet}OH$, or $O_2^{\bullet-}$ in photocatalysis. On the other hand, the adsorption decreased at higher pH values because of the repulsion between the negatively charged surface of hematite and anionic dye molecules as a result of the photodegradation efficiency of the IC declined.

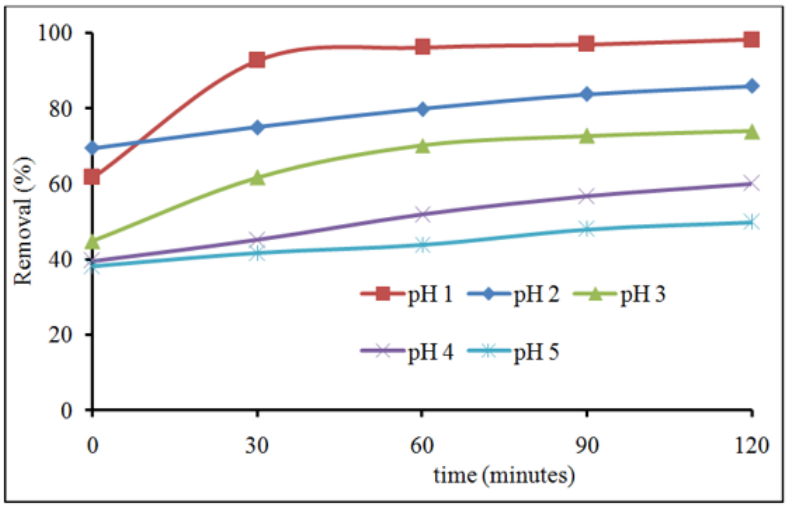

Figure 3. Photodegradation of IC over Cu-doped hematite. The initial IC concentration and photocatalyst masses are 15 mg/L and 300 mg, respectively.

The effect of photocatalyst mass on the photodegradation of IC dye was studied with different Cu-doped hematite mass ranging from 200 to 400 mg on the initial pH of the IC solution which was 1 (Figure 4). The results showed that photodegradation efficiency of the IC increased with the increase in mass of photocatalyst, which confirmed that more active sites led to the production of more reactive radicals (-$HO^{\bullet}$, $O_2^{\bullet}$), which in turn caused to higher rates of IC photodegradation [24]. The maximum photodegradation efficiency of IC (98.41 %)occurred on the maximum photocatalyst mass used in this report. Therefore, the photocatalyst mass used on the further photodegradation evaluation was performed by using 400 mg of the photocatalyst.

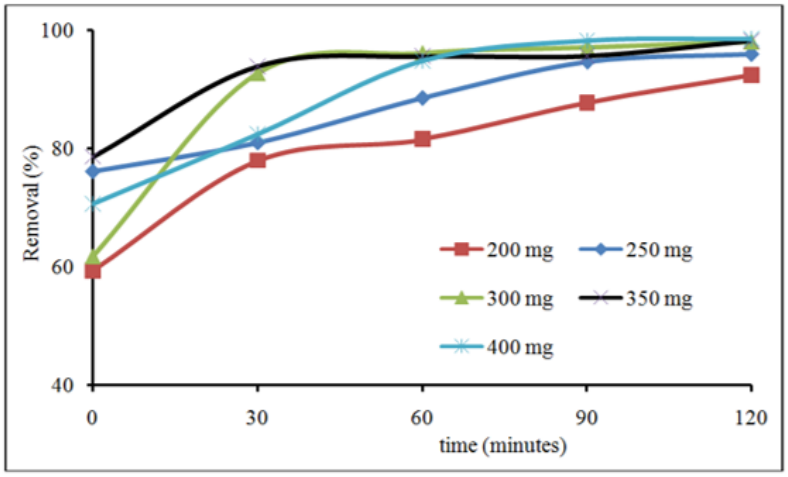

Figure 4. Photodegradation of IC over Cu-doped hematite. Initial IC concentration is 15 mg/L, initial pH of IC solution is 1

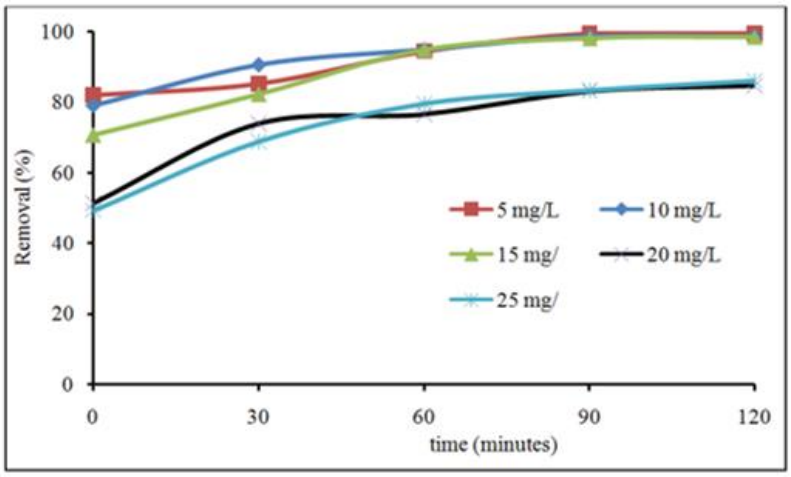

Figure 5. Photodegradation of IC over Cu-doped hematite. Initial pH of IC solution is 1 and photocatalyst mass is 400 mg

Figure 5 shows the influence of the initial concentration of IC solution on its photodegradation over Cu-doped hematite nanoparticles. Five different IC concentrations were used to evaluate the impact of the initial concentration of IC on the photodegradation while keeping constant the photocatalyst mass (400 mg). The results revealed that the photodegradation rate of IC with the initial concentration of 5 mg/L to15 mg/L was almost the same. Increasing the initial IC concentration to 20 and 25 mg/L caused the decrease in the photodegradation rate. This observation can be explained because the higher the IC concentration, the more IC molecules can react with the active site (holes, electrons or -$OH^{\bullet}$) on photocatalyst surface after being irradiated by UV light. However, at the higher IC concentration, the dye molecules prevented the UV light to reach the surface of the photocatalyst, hence decreasing the generation of electrons and holes leading to less production of reactive $-HO^{\bullet}$ on the photocatalyst surface [25-26], and lower extents of photodegradation.

Figure 6 shows the photodegradation of IC dye over different photocatalysts under UV or solar light irradiation for 90 minutes at optimum conditions (pH = 1, photocatalyst mass = 400 mg). It is evident that the doping copper ion into the crystal lattice of hematite could enhance the photocatalytic activity of hematite. The increase in photocatalytic activity of Cu-doped hematite can be arisen by the decrease in electron-hole pair recombination rate due to the copper impurity energy level which traps

electrons [27]. In addition, the specific surface area of Cu-doped hematite was higher than that of undoped hematite; as a result, the active surface available for chemical reaction increased [8]. Cu-doped hematite has high photocatalytic activity both under UV and solar light irradiation.

Figure 6 also exhibits that Cu-doped hematite is an excellent adsorbent which could remove IC up to 89.21 %. Since hematite has been widely considered as a photocatalyst, the experiment also conducted using hematite extracted from iron ore. The result showed that hematite had a higher photocatalytic activity under solar light compared with UV light irradiation but the photocatalytic activity was still lower than Cu-doped hematite. This case was probably becausethe photon energy of the UV light used in this report (at λ = 365 nm and 6 W) was less than that of solar light that contained UV A (400-320 nm), UV B (320-290 nm), and UV C (290-200 nm) [28]. The degradation of IC itself under UV and solar light could achieve 2.60 % and 10.09 % within 90 min, respectively.

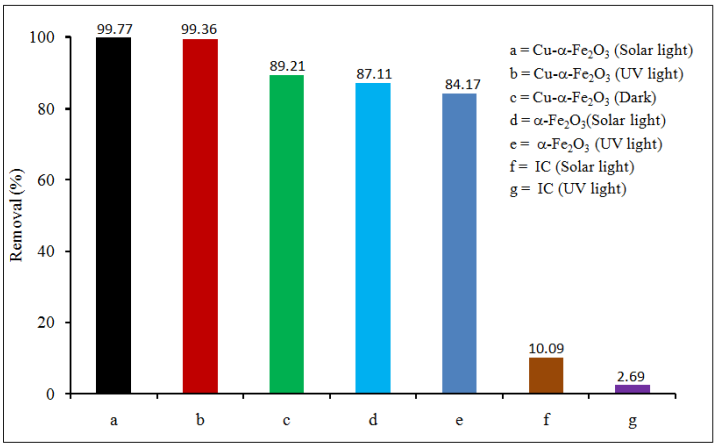

Figure 6. Photodegradation of IC in the presence of different photocatalysts under irradiation with UV and solar light. The initial pH of IC solution is 1, the initial IC concentration is 15 mg/L, and the photocatalyst mass is 400 mg

The photocatalytic activity of Cu-doped hematite was also evaluated on the photodegradation of dyes found in batik wastewater. The results showed that dyes in batik wastewater could remove up to 77.56 % and 97.83 % under UV and solar light irradiation**,** respectively.

4. Conclusion

In this study, Cu-doped hematite nanoparticle was prepared using an impregnation method and its characteristics and photocatalytic activity were investigated. The crystallite size of Cu-doped hematite was slightly smaller than that of undoped hematite. According to the nitrogen adsorption-desorption results, the specific surface area of Cu-doped hematite was higher than that of undoped hematite. The photocatalytic testing confirmed the role of copper ion doping on hematite. Photodegradation investigation showed that Cu-doped hematite had the highest photocatalytic activity on the experiment conditions: the initial pH of IC solution was 1.0; the photocatalyst mass was 400 mg; the initial concentration of IC 15 mg/L and 90 minutes irradiation times both under UV and solar light. Cu-doped hematite nanoparticles could also remove the dyes found in batik wastewater with a percentage of degradation up to 77.56 and 97.83% under UV and solar light irradiation, respectively.

Acknowledgments

The authors gratefully thank the Universitas Syiah Kuala for financial support through the PLK Research Grant number: 60/UN11.2/PP/PNBP/SP3/2018.

References

[1] Zhu J, Yin Z, Yang D, Sun, Wijayantha &, K G U, Tahir A A and Vaidhyanathan B 2009 *J. Phys. Chem. C* **113** 4768.
[2] Bouhjar F, Mollar M, Chourou M L, Mari B and Bessaïs B 2018 *Electrochim. Acta* **260** 838.
[3] Zhang M, Lin Y, Mullen T G, Lin W F, Sun L D, Yan C H, Patten T E, Wang D and Liu G Y 2012 *J. Phys. Chem. Lett.* **3** 3188.
[4] Sina S Y, Wijayantha K G U, Tahir AA and Vaidhyanathan B 2009 *J. Phys. Chem C* **113** 4768.
[5] Li X, Yu X, He J and Xu Z 2009 *J. Phy. Chem.* C **113** 2837.
[6] Sartoretti C J, Ulmann M, Alexander B D, Augustynski J and Weidenkaff A 2003 *Chem Phys. Lett.* 376 194.
[7] Mishra M and Chun D M 2015 *Appl. Catal. Gen.* **498** 126.
[8] Babi´c B, Zarubica A, Arsi´c T M, Panti´c J, Joki ´c B, Abazovi´c N and Matovi´c B 2016 *J. Eur. Ceram. Soc*. **36** 2991.
[9] Dang M Z, Rancourt D G, Dutrizac J E, Lamarche G and Provencher R 1998 *Hyperfine Interact.* **117** 271.
[10] Zysler R D, Fiorani D, Testa A M, Suber L, Agostinelli E, Godinho M 2003 *Phys. Rev. B: Condens. Matter*. **68** 212408.
[11] López J L, Pfannes H D, Paniago R, Sinnecker J P and Novak M A 2008 *J. Magn. Magn. Mater.* **320** (14) 327.
[12] Owoza D, Przewoźnik J, Kozłowski A, Kąkol Z, Wiecheć A and Honig J M 2005 *Physica B* **359-361** 1339.
[13] Suresh R, Giribabu K, Manigandan R, Mangalaraja RV, Solorza J Y, Stephen A and Narayanan V 2017 *Solid State Sci.* **68** 39.
[14] Xiao Z, Li J, Zhong J, Hu W, Zeng J, Huang S, Lu X, He J and Li M 2014 *Mater. Sci. Semicond. Process* **24** 104.
[15] Patil D. Patil V and Patil P 2011 *Sens. Actuators* B **152** 299.
[16] Cao Z, Qin M, Gua Y, Jia B, Chen P and Qu X 2016 *Mater. Res. Bull.* **77** 41.
[17] Mansour H, Bargougui R, Autret-Lambert C, Gadri A and Ammar S 2018 *J. Phys. Chem. Solids* **114** 1.
[18] Torimoto T, Okawa Y, Takeda N and Yoneyama H 1997 *J. Photochem. Photobiol. A: Chem.* **103** 153.
[19] Lekshmi K P V, Yesodharan S, Yesodharan E P, 2008 *Heliyon*e **4** 00897.
[20] Barhon Z, Bozon-Verdurac F, Saffaj N, Albizane A, Azzi M., Azzi, Kacimi M, dan Ziyad M, 2011 *Desalination and Water Treat*. **30** 69.
[21] Khokhawala I M and Gogate P R 2010 *Ultrason. Sonochem.* **17** 833.
[22] Netpradit S, Thiravetyan P and Towprayoon S 2004 *J. Colloid Interface Sci*. **270** 255.
[23] Neppolian B, Kim Y, Ashokkumar M, Yamashita H and Choi H 2010 *J. Hazard. Mater.* **182** 557.
[24] Das R, Bhaumik M, Giri S and Maity A 2017 *Ultrason. Sonochem.* **37** 600.
[25] Soltani R D C, Jorfi S, Ramezani H and Purfadakari S 2016 *Ultrason. Sonochem.* **28** 69.
[26] Khataee A, Sheydaei, M Hassani A, Taseidifar, M and Karaca, S 2015 *Ultrason. Sonochem.* **22** 404.
[27] Houas A, Lachheb H, Ksibi M, Elaloui E, Guillard C and Herrmann J M 2001 *Appl. Catal. B* **31** 14.
[28] Dong P D, Munson C A, Norton W, Crosnier C, Pan X, Gong Z, Neumann C J and Stainier D Y 2007 *Nature Genet*. **39** 397.